

# Radiative Heat Transfer Analysis in Modern Rocket Combustion Chambers

Florian Göbel\*, Björn Kniesner\*\*, Manuel Frey\*\*, Oliver Knab\*\*, Christian Mundt\*

\* *Universität der Bundeswehr München  
Institute of Thermodynamics, LRT-10  
85577 Neubiberg, Germany*

\*\* *EADS Astrium Space Transportation  
System Analysis & Modeling TP22  
81663 München, Germany*

[florian.goebel@unibw.de](mailto:florian.goebel@unibw.de), [bjorn.kniesner@astrium.eads.net](mailto:bjorn.kniesner@astrium.eads.net), [manuel.frey@astrium.eads.net](mailto:manuel.frey@astrium.eads.net),  
[oliver.knab@astrium.eads.net](mailto:oliver.knab@astrium.eads.net), [christian.mundt@unibw.de](mailto:christian.mundt@unibw.de)

## Abstract

Radiative heat transfer analyses for subscale and fullscale rocket combustion chambers with H<sub>2</sub>/O<sub>2</sub> and CH<sub>4</sub>/O<sub>2</sub> combustion are performed. The method of Spherical Harmonics (P1 radiation transport model) is used in combination with various Weighted Sum of Gray Gases Models (WSGGM) to assess the Radiative Wall Heat Flux to the walls of the combustion chamber. The influence of different wall emissivities is investigated as well as the results using different WSGGM.

For both H<sub>2</sub>/O<sub>2</sub> and CH<sub>4</sub>/O<sub>2</sub> combustion the ratio of Radiative Wall Flux to Total Wall Heat flux decreases linearly with the emissivity of the wall. Using rather simple WSGGM yields nearly the same results as using sophisticated models which is true for all combustion chamber sizes and all combustion reactions investigated.

The local ratio of Radiative Wall Heat Flux to Total Wall Heat Flux shows a maximum of 9-10 % for H<sub>2</sub>/O<sub>2</sub> combustion near the injector which is therefore influenced most by radiation. The integrated ratio is around 3 % for that propellant combination. For CH<sub>4</sub>/O<sub>2</sub> combustion, due to a slightly lower combustion temperature of the considered load point, the maximum local flux ratio decreases to 8 % whilst its location is still at the inlet. Consequently, the integrated ratio of Radiative Wall Heat Flux to Total Wall Heat Flux decreases to a maximum of 2.5 %.

## Nomenclature

### Latin Symbols:

$a$	= Absorption coefficient
$C$	= Absorption cross section
$\bar{C}$	= Mean Absorption cross section
$f$	= Mixture fraction
$h_q$	= Reduced enthalpy
$F$	= Blackbody distribution function
$G$	= Incident radiation
$i$	= Radiation intensity
$I$	= Number of gray gases
$\vec{n}$	= Normal vector
$q$	= Heat flux
$r$	= Function of mixture
$S$	= Path length

$w$  = Blackbody weight of gray gas

### Greek Symbols:

$\epsilon$	= Surface emissivity
$\phi$	= Scattering phase function
$\sigma$	= Scattering coefficient Stefan-Boltzmann constant
$\omega$	= Solid angle

### Subscripts:

b	= Blackbody property
c	= Carbon dioxide
i	= Index of gray gas Numeration index

j	= Numeration index	CWHF	= Convective Wall Heat Flux
mix	= Mixture	NSMB	= Navier Stokes Multiblock
min	= Minimum	RTE	= Radiative Transfer Equation
max	= Maximum	PPDF	= Presumed Propability Density Function
w	= Water vapour	RWHF	= Radiative Wall Heat Flux
$\lambda$	= Spectral value	SSME	= Space Shuttle Main Engine
Abbreviations and Acronyms:		TWHF	= Total Wall Heat Flux
CFD	= Computational Fluid Dynamics	WSGGM	= Weighted Sum of Gray Gases Model

## 1. Introduction

Heat transfer analysis is crucial during the design process of rocket combustion chambers since the development of cooling systems and hence the life time of those chambers highly depends on the occurring heat loads. With their gas temperatures above 3000 K rocket combustion chambers are likely influenced by radiative heat transfer that depends on temperature's fourth power.

The analysis of radiative heat transfer is a very complicated part of heat transfer calculations as it requires the solution of the Radiative Transfer Equation (RTE) which depends on spatial, directional and spectral variables. Analytical solutions for the RTE have been achieved only for simplified cases whereas for most other applications numerical approximations are used to solve the RTE.

One of these numerical approximations is the P1 radiation model or Method of Spherical Harmonics which simplifies the RTE by taking an angularly averaged intensity leading to a four dimensional partial differential equation that depends only on spatial and spectral variables. The spectral dependencies can then be simplified using so called Spectral Models from which one is the Weighted Sum of Gray Gases Model (WSGGM) that has been improved by several authors in the past [1, 2, 3, 4].

The P1 radiation models and the WSGG models of those authors have been implemented into the CFD code NSMB [5] at the Institute of Thermodynamics of the University of the Armed Forces. Both models have been validated with simple cases for which analytical solutions of the RTE exist [6]. Within that work, both models have also been applied to the analysis of radiative heat transfer in the Space Shuttle Main Engine (SSME).

Former investigations by Naraghi [7], Wang [8], Thellmann [9] and Goebel [6] concluded that for  $H_2/O_2$  combustion integrated radiative heat loads to the wall have a share of nearly 8 % on the total heating of the wall whilst the local flux ratio exceeds 30 %. Assuming thrust-identity for a fictitious  $CH_4/O_2$  combustion in the Space Shuttle Main Engine Thellmann [9] and Goebel [10] have shown that radiation's integrated share on the Total Wall Heat Flux (TWHF) increases to nearly 9 %.

Nevertheless, one of the shortcomings of these investigations is that the flow field of the SSME was predicted by CFD codes not taking into account the effects of propellant preparation on the heat load development especially in the injection region, which leads to an overestimation of the temperature field and hence the integral gas radiation contribution.

The aim of this work is therefore to assess radiative heat loads on the wall of various combustion chambers that are part of EADS Astrium's portfolio. As basis, more reliable flow field predictions by Astrium's in-house spray combustion CFD code Rocflam-II are used, which are validated against numerous experiments [11], taking into account propellant preparation effects such as propellant disintegration, evaporation and mixing.

By using subscale and fullscale combustion chambers for  $H_2/O_2$  and a subscale chamber for  $CH_4/O_2$  combustion, the influence of a  $H_2O/CO_2$  mixture on the Radiative Wall Heat Flux (RWHF) is investigated in comparison to single  $H_2O$  systems.

For these analyses, the P1 radiation model of NSMB in conjunction with the WSGG models mentioned above are employed. Results for the temperature, pressure and mole fractions of  $H_2O$  and  $CO_2$  are imported from Rocflam-II into NSMB which calculates the parameters for the WSGGM and afterwards solves the P1 radiation transport equations. This is done in an uncoupled manner, meaning that the influence of radiation on the energy conservation inside the combustion chamber is neglected.

The results in RWHF are compared to the Convective Wall Heat Flux (CWHF) for both  $H_2/O_2$  and  $CH_4/O_2$  combustion. The influence of wall emissivities and WSGG models is examined using the RWHF and its ratio to the TWHF, being the sum of RWHF and CWHF. The local ratio of RWHF to TWHF is investigated for both chambers and their corresponding propellant combination, yielding a qualitative overview of those regions in the combustion chambers that are influenced most by the RWHF. The integrated ratio of RWHF to TWHF finally gives the mean influence of radiation on the total heat loads.

## 2. Numerical Method

### 2.1 Theory of Radiative Transfer

The Radiative Transfer Equation (RTE) in its spectral form is the basis of all radiative heat transfer investigations, [12, p. 562]

$$\frac{di_\lambda}{dS} = a_\lambda \cdot i_{\lambda b} - (a_\lambda + \sigma_\lambda) \cdot i_\lambda + \frac{\sigma_\lambda}{4\pi} \cdot \int_{4\pi} i_\lambda \cdot \phi_\lambda(\omega_i, \omega) d\omega_i. \quad (1)$$

The RTE in Eq. (1) describes the change of a beam's intensity passing through a radiatively participating medium in the direction  $s$ . The change is due to a gain of intensity by emission and scattering and a loss of intensity by absorption and scattering. The RTE is an integro-differential equation depending on 3 spatial, 2 directional and 1 spectral variable, which makes an analytical solution almost impossible for most engineering applications. Thus, it has to be solved numerically using radiation transport models for spatial and directional dependencies and spectral models for the spectral dependency. One of the radiation transport models is the P1 Radiation Model or the method of Spherical Harmonics. One of the spectral models is the Weighted Sum of Gray Gases Model (WSGGM) that is used to reduce the numerical effort of spectral integration.

### 2.2 Governing Equations of the P1 Radiation Model

One way to simplify the Radiative Transfer Equation (RTE) is the method of Spherical Harmonics. In this method, the radiative intensity is approximated by a two-dimensional Fourier-series, splitting the intensity's spatial and directional dependency. If the Fourier-series is truncated after one element, the so-called P1 Radiation Model is achieved. In the following parts, scattering of radiation is neglected since production of soot etc. is not considered in this work. A detailed derivation of the Spherical Harmonics method can be found in [13, p. 466].

The P1 Radiation Model yields two spatial differential equations, one for the gradient of the directionally averaged intensity  $G_\lambda$

$$\bar{q}_{\text{rad},\lambda} = -\frac{1}{3a_\lambda} \nabla G_\lambda, \quad (2)$$

and another for the gradient of the radiative heat flux  $\bar{q}_{\text{rad},\lambda}$

$$\nabla \bar{q}_{\text{rad},\lambda} = a_\lambda (4\pi i_{\lambda b} - G_\lambda), \quad (3)$$

which can be combined to a second order partial differential equation of elliptic type

$$\nabla \left( \frac{1}{3a_\lambda} \nabla G_\lambda \right) = a_\lambda (G_\lambda - 4\pi i_{\lambda b}), \quad (4)$$

that is subject to the boundary condition at a solid wall

$$G_\lambda - \frac{2}{3a_\lambda} \left( \frac{2 - \varepsilon_{\lambda w}}{\varepsilon_{\lambda w}} \right) \nabla G_\lambda \cdot \vec{n}_w = 4\pi i_{\lambda bw}. \quad (5)$$

The P1 Radiation Model has been implemented in the research CFD code NSMB [5] using a local time stepping algorithm and validated against simple test cases for which analytical solutions are available [6].

### 2.3 Spectral Modeling: Weighted Sum of Gray Gases Model (WSGGM)

Integration of the RTE over wavelength often leads to extreme efforts when using Line-by-Line spectral data because the RTE has to be solved for each spectral line. To overcome this problem, spectral models like the WSGGM are used. Further details on the theory of the WSGGM and some of the up-to-date models can be found in [14] as well as detailed derivation of the WSGGM approach.

The simplifying approach of the WSGGM is to subdivide the entire spectrum into regions in which the absorption coefficient is assumed to have a constant value  $a_i$ . As the absorption coefficient is no longer dependent on the wavelength in this region, it fulfils the requirements of a gray gas, which gives the model its name. Additionally to the gray gases, those regions in the spectrum in which no absorption occurs are represented by a clear gas denoted by index  $i=0$  with  $a_0=0$ .

In the WSGGM, integration over wavelength is replaced by a weighted sum over all gray gases. The spectrally integrated property is then the sum of all gray gases' properties. The governing equation of the P1 model of Eq. (4) becomes

$$\nabla \left( \frac{1}{3a_i} \nabla G_i \right) = a_i (G_i - 4\pi w_i i_{i,b}). \quad (6)$$

The boundary condition of Eq. (5) becomes

$$G_i - \frac{2}{3a_i} \left( \frac{2 - \varepsilon_w}{\varepsilon_w} \right) \nabla G_i \bar{n}_w = 4w_{i,w} \sigma T_w^4, \quad (7)$$

with the wall's blackbody weight  $w_{i,w}$  and the wall temperature  $T_w$ . The blackbody weight  $w_i$  indicates the fraction of the entire blackbody spectrum in which the absorption coefficient is  $a_i$

$$w_i = \frac{i_{i,b}}{\int_0^\infty i_\lambda d\lambda} = \frac{i_{i,b}}{\left( \frac{\sigma T^4}{\pi} \right)}. \quad (8)$$

Note that if the weight  $w_i$  is a function of temperature, the temperature of the wall has to be used for the wall's blackbody weight  $w_{i,w}$ . The WSGG models currently implemented in NSMB are those by Smith [1] for H<sub>2</sub>O and H<sub>2</sub>O/CO<sub>2</sub> mixtures, by Copalle [2] and Johansson [4] for H<sub>2</sub>O/CO<sub>2</sub> mixtures and by Denison & Webb [15, 16] for H<sub>2</sub>O and H<sub>2</sub>O/CO<sub>2</sub> mixtures. The first three use a rather simple approach to gain absorption coefficients and weights from total emissivity curve fits whereas the latter model is based on spectral databases.

For mixtures of H<sub>2</sub>O and CO<sub>2</sub>, the numerical effort remains the same as for single H<sub>2</sub>O systems except for the model of Denison & Webb. While the models of Smith, Copalle and Johansson employ the same number of gray gases  $I$  for those mixtures (Smith:  $I=3$ , Copalle:  $I=3$ , Johansson:  $I=4$ ), there are several options for Denison & Webb's model. The first option, known as double-integration, calculates the mixture absorption coefficients and weights according to

$$w_{w,c} = w_w w_c = \left[ F_w(C_{w,j+1}) - F_w(C_{w,j}) \right] \left[ F_c(C_{c,j+1}) - F_c(C_{c,j}) \right], \quad (9)$$

$$a_{w,c} = N_w \bar{C}_{w,j} + N_c \bar{C}_{c,j}. \quad (10)$$

The mean absorption cross section of each species is defined as

$$\bar{C}_j = (C_j C_{j+1})^{1/2}. \quad (11)$$

The disadvantage of this option is that the number of gray gases and thus the number of equations to be solved is exponentiated, e.g. when using  $I=10$  gray gases for each species, the total number of gray gases becomes  $(I+1) \times (I+1) = 121$  which is a huge amount of additional computational effort. One possibility to lower the computational efforts is to use less than 10 gray gases per radiating species with the double integration which in turn requires an optimization technique as suggested by Denison & Webb [3]. In this work, reduction to 3 gray gases per species is investigated, leading to a total number of 16 gray gases.

The second option is called convolution approach. In contrast to the double-integration, this option needs only  $I$  gray gases, similar to the single species system. At first, 10 values for  $\bar{C}_{\text{mix},j}$  are defined from which the absorption coefficient is yielded from

$$a_{w,c} = (N_w + N_c) \bar{C}_{\text{mix},j}. \quad (12)$$

The weight is obtained by subtracting two contiguous blackbody distribution functions

$$w_{w,c} = \left[ F_{\text{mix},j+1}(C_{\text{mix},j+1}) - F_{\text{mix},j}(C_{\text{mix},j}) \right], \quad (13)$$

with

$$F_{\text{mix},j}(C_{\text{mix},j}) = \int_{F_c(C_{c,\text{min}})}^{F_c(C_{c,\text{max}})} F_w \left( \frac{C_{\text{mix},j} - rC_c}{1-r} \right) dF_c(C_c), \quad (14)$$

$$r = \frac{N_c}{N_w + N_c} \quad (15)$$

and

$$C_{c,\text{max}} = \left( \frac{C_{\text{mix},j} - (1-r)C_{w,\text{min}}}{r} \right). \quad (16)$$

$C_{w,\text{min}}$  and  $C_{c,\text{min}}$  are chosen as  $3 \cdot 10^{-5} \text{ mol}^{-1}$  and  $C_{c,\text{max}}$  is set to  $60 \text{ mol}^{-1}$ . The integration of Eq. (14) is carried out with a Gaussian quadrature over 60 intervals. Due to the well behaved characteristics of  $F_{\text{mix},j}(C_{\text{mix},j})$  this method is expected to yield a satisfying accuracy with least efforts. The number of intervals has been optimized to 60 within various tests, yielding an error of below 0.5 % to the solution with 1000 intervals that would lead to much more computational efforts [17].

The disadvantage of this model is its limitation to systems with a constant mole fraction of species which does not apply to the combustion chambers in this work. The model is therefore used beyond its limitations with variable mole fractions.

## 2.4 Numerical method for the basic flow

For the basic flow (velocity, pressure and temperature field, gas properties and composition) inside the considered combustion chambers, Astrium's in-house CFD code Rocflam-II is used [18]. Rocflam-II is an axisymmetric Navier-Stokes solver with a Lagrange droplet tracking module that incorporates several models for multi-class droplet tracking, evaporation and combustion, balancing their accuracy and computational effort.

The turbulence modeling is realized via a two-layer  $k-\varepsilon$  model which switches to a one-equation model for the turbulent kinetic energy near the wall, determining the dissipation  $\varepsilon$  from an algebraic expression. For the propellant combinations  $\text{H}_2/\text{O}_2$  and  $\text{CH}_4/\text{O}_2$  an equilibrium-table-based chemistry model is used with a one-dimensional PPDF (Presumed Probability Density Function) approach taking into account the influence of turbulent combustion. No species concentration equations are solved, only a global mixture fraction and its variance are treated by differential equations.

The key of this type of combustion model is the combustion table which is computed separately prior to the computation itself by a chemical equilibrium code and a fluid database. A visualization of the chemistry tables for  $\text{CH}_4/\text{O}_2$  and  $\text{H}_2/\text{O}_2$  are given in Fig. 1. The temperature evolution of the combustion between fuel and oxygen is shown as contour on the  $z$ -axis and additionally as contour color. On the other axes the gas solver input quantities mixture fraction  $f$  and reduced enthalpy  $h_q$  are shown. Here,  $f=1$  ( $O/F=0$ ) means pure fuel,  $f=0$  ( $O/F \rightarrow \infty$ ) represents pure oxygen. The stoichiometric mixtures of  $f \approx 0.2$  ( $O/F \approx 4$ ) for  $\text{CH}_4/\text{O}_2$  and  $f \approx 0.112$  ( $O/F \approx 8$ ) for  $\text{H}_2/\text{O}_2$  are indicated by the red arrows. The enthalpy level of zero corresponds to the injection

temperature of fuel and oxidizer at  $f = 1$  and  $f = 0$  respectively. Positive enthalpy is related to higher, negative enthalpy is related to lower temperatures. At the stoichiometric ratio the temperature is maximal for the given enthalpy level. It is clearly visible that the combustion temperature increases with increasing enthalpy and pressure. The tables are multi pressure tables which are necessary for a correct description of the flow and the combustion over the entire computational domain including throat and nozzle where the pressure strongly decreases due to flow expansion. The effect of different pressure levels in the table is visible by the multiple contour layers. With increasing pressure, dissociation becomes weaker resulting in a higher temperature at high pressure levels.

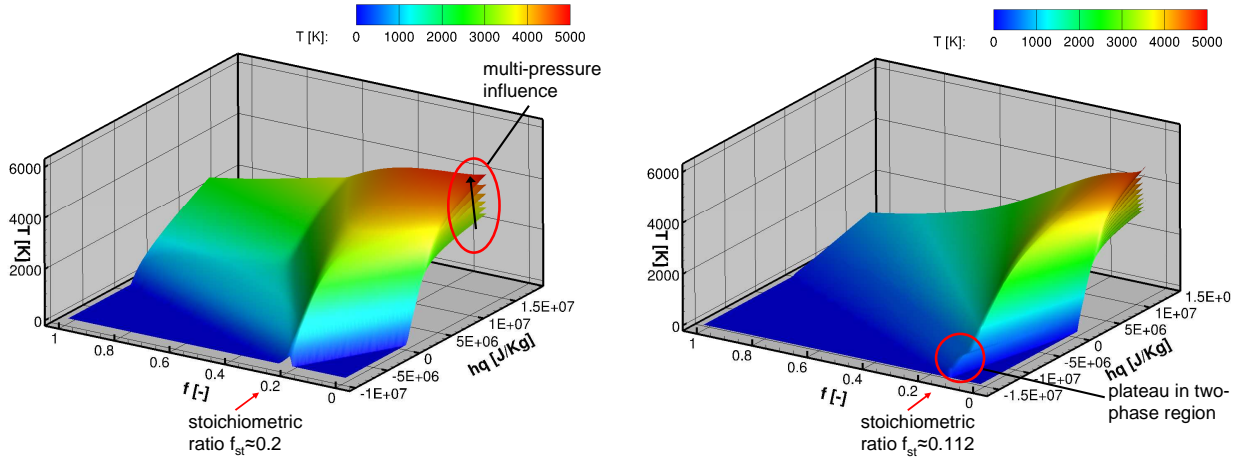


Figure 1: Multi-pressure equilibrium chemistry table for  $\text{CH}_4/\text{O}_2$  (left) and  $\text{H}_2/\text{O}_2$  combustion (right) [19].

### 3. Calculation Strategy

In Fig. 2 the calculation sequence of this work is shown. Based on the Rocflam-II results for temperature, pressure and mole fraction of radiating species imported into NSMB, a routine in NSMB calculates the WSGGM properties absorption coefficient and blackbody weight for each gray gas. These are used as input to the routine that solves the P1 radiation transport model yielding the incident radiation  $G_i$  for each gray gas. With a converged solution of the P1 radiation model, postprocessing routines in NSMB construct the RWHF.

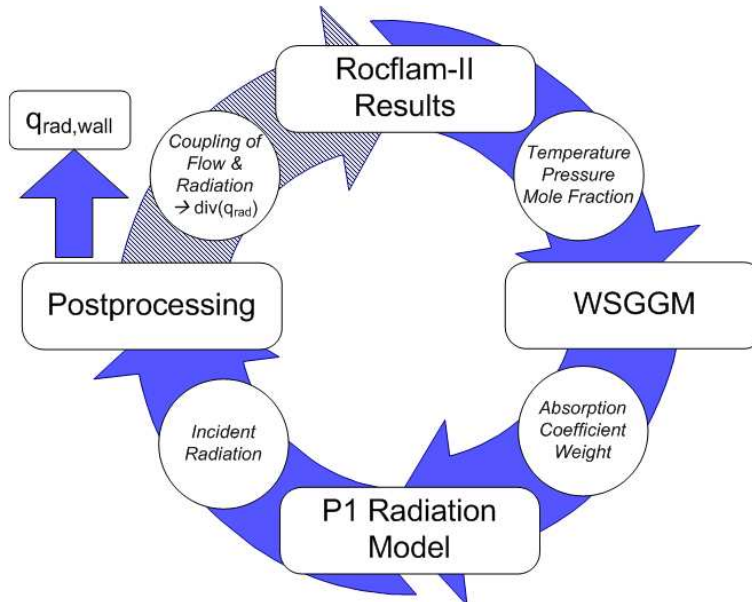


Figure 2: Calculation sequence for Radiative Heat Transfer Analysis

As a further option, the divergence of the total radiative heat flux can be used as input to Rocflam-II in a loosely coupled calculation. For loosely coupled simulations, the divergence of the total radiative heat flux, which is the sum

over all gray gases, has to be added to the energy equation of Rocflam-II to account for energy transport by radiation, yielding a modified flow field which is then used as input for another radiation simulation. The loose coupling procedure is done until convergence is reached. Coupling is left out in this work which is indicated by the dashed arrow in Fig. 2, but will be reported in the near future.

#### 4. H<sub>2</sub>/O<sub>2</sub> Combustion

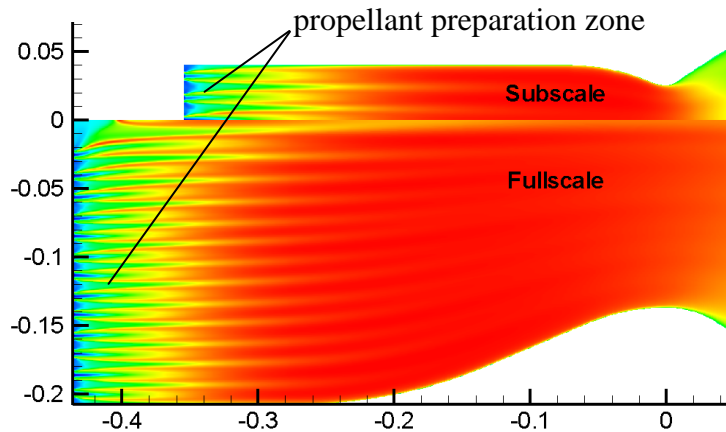


Figure 3: Temperature contours of Subscale and Fullscale Combustion Chamber for H<sub>2</sub>/O<sub>2</sub> combustion

For the H<sub>2</sub>/O<sub>2</sub> combustion two different geometries are investigated, a subscale and a fullscale chamber [3]. The subscale design has been chosen in a way that it is representative for fullscale in terms of heat load on the wall as well as characteristic length and thus propellant preparation and evaporation. The smaller dimensions of the subscale hardware make it possible to experimentally gather detailed calorimetric heat flux measurements. The calorimetric measurements are realized by computing the enthalpy difference between inflow and outflow of the multiple individual segments on the basis of temperature, pressure as well as velocity differences. The comparison of these data to the Rocflam-II simulation is presented in Figure 4.

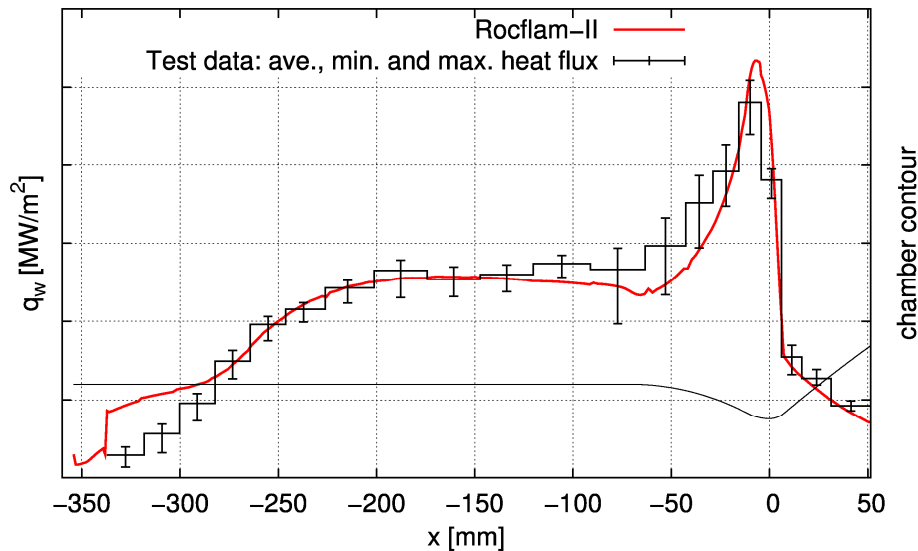


Figure 4: Local heat flux profiles of simulation and experiment for the H<sub>2</sub>/O<sub>2</sub> Subscale chamber

It becomes visible that the overall agreement between simulated and measured local heat flux is very good. A small deviation can be observed in the injection area near the face plate, where the simplification of axisymmetry has its strongest influence. Both, the temperature plot in Fig. 3 as well as the heatflux profile in Fig. 4 display the propellant preparation zone which has not been resolved in former studies [9, 10] providing a combustion efficiency lower than

unity and a thermally less loaded region close to the injector. The load point (chamber pressure and mixture ratio) for which the comparison is shown matches the load point of the fullscale chamber. Due to the chosen similarity of full- and subscale and the comparable load point it is expected that the local heat flux prediction by the simulation presents a realistic evolution also for the fullscale chamber. This is confirmed by the good agreement of the integral heat load between simulation and experiment for the fullscale chamber. There, the measurement of the integral heat load is realized by a single calorimetric measurement between inlet and outlet of the cooling circuit.

The results in RWHF for both the subscale and fullscale combustion chamber using different wall emissivities can be seen in Fig. 5. The plots are normalized with the maximum CWHF of the corresponding combustion chamber. The left and the right scale of each diagram in Fig. 5 differ by two orders of magnitude; at intersections of RWHF and CWHF the former is 1 % of the latter. Additionally, the radially averaged temperature is shown in Fig. 5.

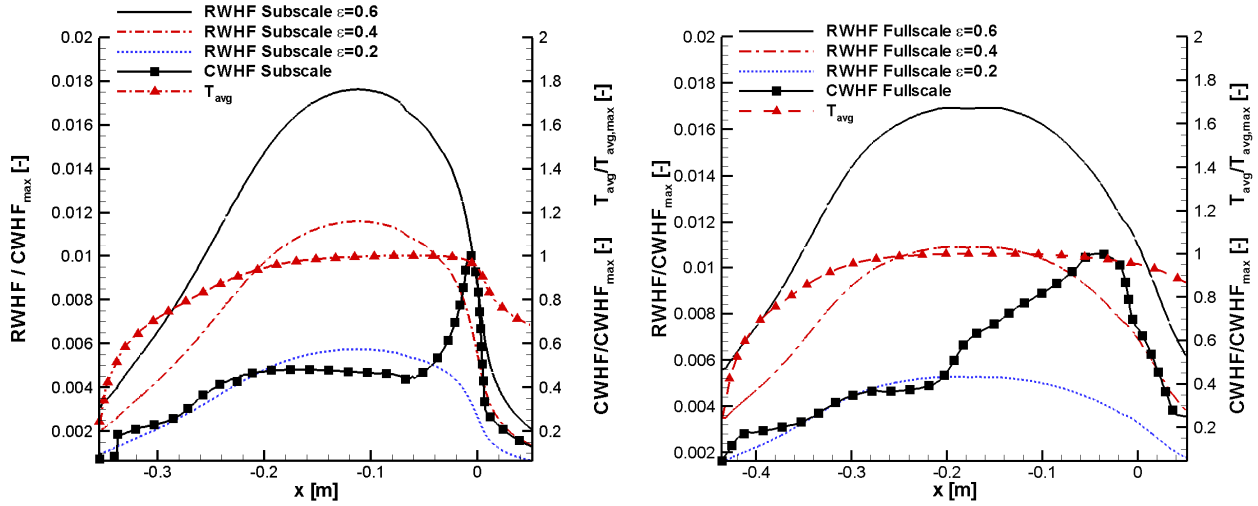


Figure 5: Normalized CWHF, RWHF and averaged temperature for Denison's WSGGM for Sub (left)- and Fullscale (right) Combustion Chamber using different wall emissivities

Firstly, one can see that the RWHF evolves with increasing temperature depending on its fourth power. As Fig. 5 underlines, the cross sectionally averaged temperature increases as chemical reactions take place, reaching its maximum shortly upstream of the throat. The RWHF also has its maximum near that position. In the subscale combustion chamber the maximum RWHF is located slightly upstream (-0.111 m) of the maximum temperature (-0.072 m) having a difference of 39 mm. In the fullscale chamber the maximum temperature lies at -0.169 m and the maximum RWHF is at -0.197 m so the difference is 28 mm. Compared to the total dimensions of the chambers the distance between the positions of maximum temperature and RWHF is 8.6 % and 5.6 % of the total chamber length. The reason for the slight difference of the maximum positions is that the radially averaged temperature has a different maximum position than those specific regions in radial direction that influence the RWHF most through their emission. Downstream of the throat the RWHF decreases rapidly with the expansion of the flow diminishing the temperature. One can see the different decreasing characteristics between the sub- and fullscale chambers downstream of the throat as the RWHF has a steeper slope in the subscale chamber. According to Fig. 5, the averaged temperature decreases more rapidly in the subscale chamber, causing the RWHF to drop off steeper than in the fullscale chamber. This is due to the fact that at equivalent nozzle length the expansion ratio of the subscale chamber is much higher than for the fullscale one.

Secondly, the influence of the wall emissivities becomes obvious in Fig. 5. With an emissivity of  $\varepsilon=0.6$  the normalized RWHF reaches its maximum of 0.0176 in the subscale and 0.0169 in the fullscale chamber. At  $\varepsilon=0.4$  it is 0.0116 and 0.0108 and with an emissivity of  $\varepsilon=0.2$  it reaches the smallest values of 0.0057 and 0.0052. Thus, the decrease in maximum RWHF is linear to the decrease in the emissivity of the wall. For the considered combustion chamber material the values can range from  $\varepsilon\approx 0.1$  for the polished case up to  $\varepsilon\approx 0.8$  for oxidized conditions. Thus, a value of  $\varepsilon=0.6$  represents a high but realistic choice, all the more when considering already aged chambers.

Thirdly, Fig. 5 shows the different length of the high RWHF zones which are broader in the fullscale combustion chamber. This difference is due to the temperature inside the chambers as Fig. 5 underlines with the averaged temperature. Because of the increased length of the fullscale combustion chamber, the high temperature regions inside this chamber are longer than in the subscale combustion chamber showing a significant region of constant maximum temperature that in turn results in a broadening of the associated high RWHF zones.

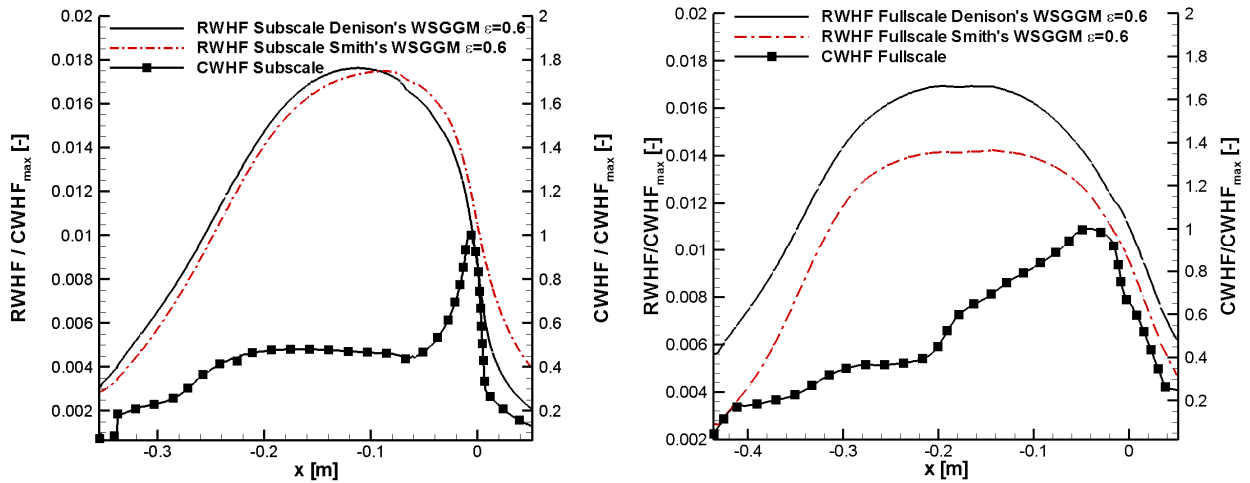


Figure 6: Comparison of normalized RWHF for Denison's and Smith's WSGGM for Sub- and Fullscale Combustion Chamber

The result of both WSGG models used in the  $H_2/O_2$  combustion, namely the ones by Smith and Denison, is shown in Fig. 6. In the subscale chamber, both WSGG models predict nearly the same ascent of the RWHF downstream of the injector as well as nearly the same maximum RWHF. Downstream of the throat the difference between both models increases. The location of the maximum RWHF is slightly shifted by 30 mm with the maximum predicted by Denison's model being upstream of the prediction by Smith's model.

For the fullscale chamber the difference between both models increases as Smith's model predicts a smaller RWHF than Denison's. The difference in maximum RWHF is around 20 %. The location of the maximum RWHF is predicted equally by both models.

Since the difference in maximum RWHF predicted by the two homogeneous WSGGM does not occur in the subscale chamber, the size of the combustion chamber seems to be responsible for that. In former investigations of the Space Shuttle Main Engine [9, p.73], whose dimensions are comparable to the fullscale chamber in this work, the WSGGM by Denison also predicted the highest RWHF compared to the simple model by Smith. With an increased dimension, especially with an increased diameter, the path length for radiative heat transfer increases and the product of absorption coefficient times path lengths grows, leading to a higher emissivity. Since Denison's model has a more profound theoretical basis than Smith's model, it is concluded that absorption is more precisely modeled in that model while Smith's model underestimates the absorption coefficient along the path, reducing the emissivity and leading to a lower maximum RWHF. The differences become obvious only in the fullscale chamber whose diameter is about 5-times the diameter of the subscale combustion chamber; the path lengths in the subscale chamber are obviously too low to cause any significant difference in maximum RWHF.

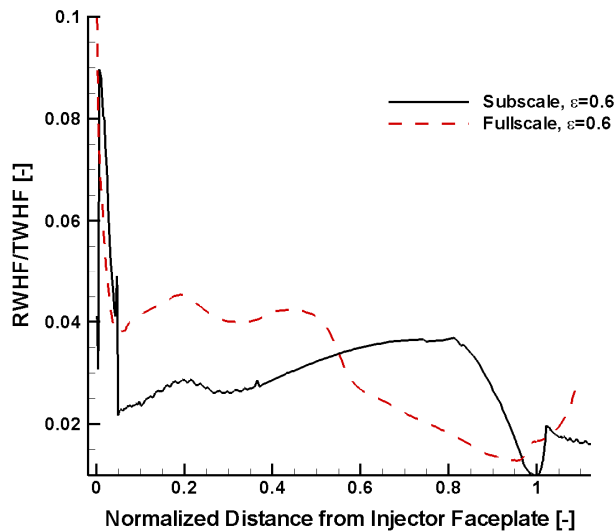


Figure 7: Local influence of RWHF on the TWHF for  $H_2/O_2$  combustion with Denison's WSGGM

Figure 7 finally summarizes the local ratio of RWHF to TWHF for both combustion chambers for the same WSGGM and constant wall emissivity. Due to the different lengths of both combustion chambers the abscissa is normalized so the position of the faceplate equals zero and the throat is at 1.0. For  $\varepsilon=0.6$  the maximum local ratio of RWHF to TWHF is nearly 10 % in the fullscale chamber and 9 % in the subscale chamber. The main reason for that high ratio is the low CWHF near the injector as predicted by Rocflam-II and confirmed by the experiments. Although the RWHF is also lowest in this region, the small CWHF causes the ratio of both to increase. Downstream of the injector the temperature and thus the RWHF and CWHF increase, with the CWHF increasing stronger than the RWHF, causing the local ratio to drop. Throughout the rest of the combustion chamber, the ratio stays below 4 %.

Table 1: Integral ratio of RWHF/TWHF for all WSGG Models, wall emissivities and chamber sizes for  $H_2/O_2$  combustion

<i>Subscale Chamber</i>	<i>RWHF/TWHF [%]</i>		
	$\varepsilon=0.6$	$\varepsilon=0.4$	$\varepsilon=0.2$
Smith's WSGGM	2,98	1,91	0,94
Denison's WSGGM	2,94	1,95	0,97
<i>Fullscale Chamber</i>	<i>RWHF/TWHF [%]</i>		
	$\varepsilon=0.6$	$\varepsilon=0.4$	$\varepsilon=0.2$
Smith's WSGGM	2,54	1,66	0,82
Denison's WSGGM	3,30	2,10	1,00

In Table 1 the integrated ratios of RWHF to TWHF are summarized. Again, one can recognize the influence of the wall emissivity on the results. The integrated ratio decreases linearly by nearly one percentage point in the subscale chamber for an emissivity decrease of 0.2. In the fullscale chamber the decrease is slightly lower with only 0.9 percentage points for each emissivity decrease of 0.2. For the subscale combustion chamber Table 1 underlines that there is nearly no difference in the prediction of both WSGG models. The biggest difference between both models is 0.04 percentage points which is less than 3 %.

In the fullscale chamber, the prediction of the integrated ratio of RWHF to TWHF differs for both WSGG models. Denison's model yields the highest ratio due to its prediction of the highest RWHF in the fullscale chamber. The maximum difference to Smith's model is 0.76 percentage points for an emissivity of  $\varepsilon=0.6$  which decreases to a minimum of 0.18 percentage points at  $\varepsilon=0.2$ . This difference is caused by the different accuracy of both models as stated above.

## 5. $CH_4/O_2$ Combustion

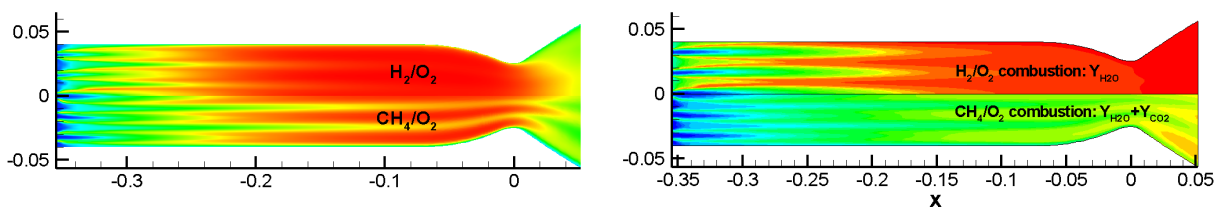


Figure 8: Temperature contours (left) and contours of mass fractions of the radiation-relevant species (right) in the Subscale Combustion Chamber for  $H_2/O_2$  and  $CH_4/O_2$  combustion

Concerning the basic flow, significant differences can be observed between hydrogen and methane combustion as Fig. 8 underlines. First of all looking at the temperature on the left of Fig. 8 it appears that the flame zone within the chamber starts farther downstream for methane than in the case of hydrogen. Furthermore, the stratification in the throat area is perceptibly higher for  $CH_4/O_2$  combustion. Both effects are mainly driven by the different droplet size distributions of the two propellant combinations.

Additionally, by looking at the right of Figure 8 one observes that the sum of mass fractions for  $H_2O$  and  $CO_2$  is significantly lower in the case of methane than it is for sole  $H_2O$  in the pure hydrogen combustion. This is surprising at first sight but results from the fact that a substantial part of the exhaust gas contains  $CO$  which is produced at high temperatures. However,  $CO$  is not considered in the radiative transfer calculation since the WSGG models used herein do not support it. Future work will clarify the effect if  $CO$  is not considered.

A comparison of the locally measured heat flux for the  $\text{CH}_4/\text{O}_2$  case in Fig. 9 shows that the general agreement with the simulation is as good as in the case of  $\text{H}_2/\text{O}_2$ .

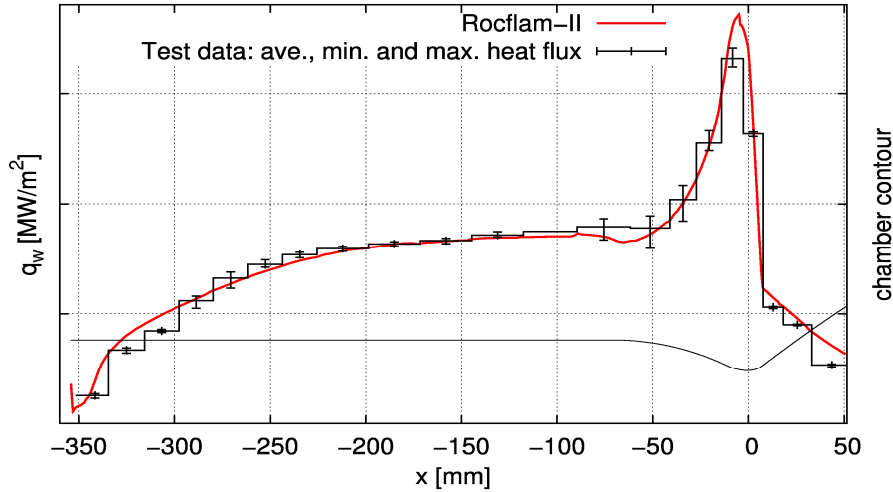


Figure 9: Local heat flux profiles of simulation and experiment for the  $\text{CH}_4/\text{O}_2$  Subscale chamber

Concerning the general evolution of the heat flux profiles it should be mentioned that the applied propellant injection method is slightly different for both propellant combinations, leading to a negligible steeper heat flux gradient in proximity of the faceplate compared to the  $\text{H}_2/\text{O}_2$  case. More important than the injection method is the load point equivalence between the two propellant combinations. Therefore, the chamber pressure for both cases is kept constant. Due to the different stoichiometric ratios of  $\text{H}_2/\text{O}_2$  ( $\approx 8$ ) and  $\text{CH}_4/\text{O}_2$  ( $\approx 4$ ) combustion the absolute value of the mixture ratio could not be kept. However, based on the available experimental data the best possible relative match to the hydrogen case was chosen. Finally, the resulting combustion temperature assuming equilibrium is about 40 K lower for the methane configuration, which has to be kept in mind when comparing the results.

Figure 10 shows the normalized RWHF in comparison with the CWHF for different wall emissivities using Smith's WSGGM. Similar to the  $\text{H}_2/\text{O}_2$  case the scales of both axes differ by approximately 2 orders of magnitude. The maximum RWHF in case of the  $\text{CH}_4/\text{O}_2$  simulation is 1.65 % of the maximum CWHF which is slightly lower than in the  $\text{H}_2/\text{O}_2$  simulation. The reason for that is on the one hand the decreased temperature of the  $\text{CH}_4/\text{O}_2$  combustion load point and on the other hand the sum of mass fractions of  $\text{H}_2\text{O}$  and  $\text{CO}_2$  which is lower than the mass fraction of pure  $\text{H}_2\text{O}$  in the  $\text{H}_2/\text{O}_2$  combustion as Fig. 8 underlines. The maximum RWHF lies 43 mm upstream of the maximum temperature which is a difference of 11 % of the total chamber length and comparable to the difference between both maxima in the  $\text{H}_2/\text{O}_2$  combustion

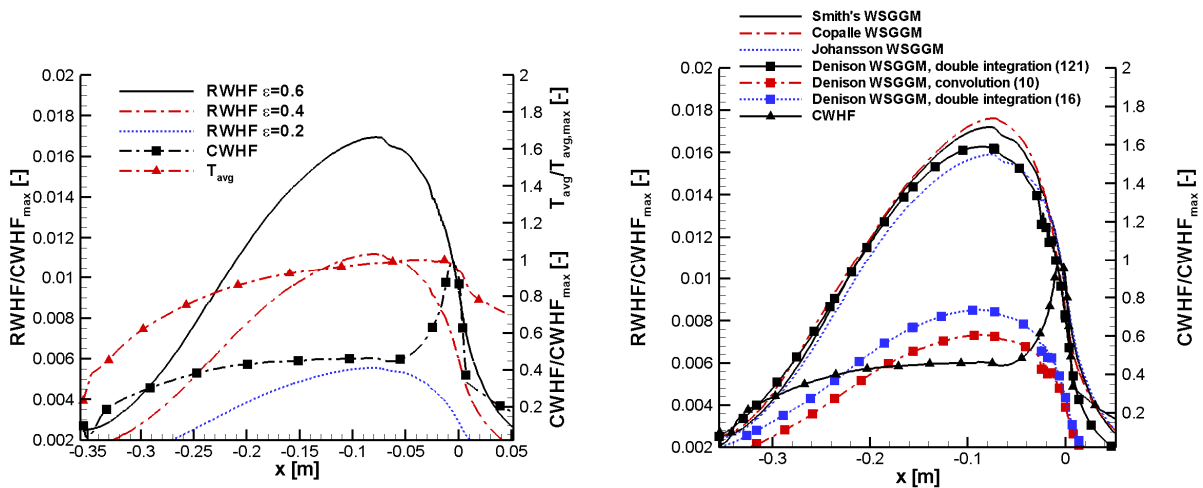


Figure 10: Normalized CWHF and RWHF for Smith's WSGGM using different wall emissivities (left) and normalized RWHF for various WSGG Models (right) for Subscale  $\text{CH}_4/\text{O}_2$  combustion ( $\epsilon=0.6$ )

With varying wall emissivity the normalized RWHF decreases from 0.0144 at  $\varepsilon=0.6$  to 0.0094 at  $\varepsilon=0.4$  and reaches its lowest value of 0.0047 with  $\varepsilon=0.2$ . Thus, the decrease in maximum RWHF with emissivity is linear like in the  $\text{H}_2/\text{O}_2$  case.

The differences in RWHF for the different WSGG models are shown in Fig. 10. Due to the presence of  $\text{CO}_2$ , in addition to the simple model by Smith that has been used for the  $\text{H}_2/\text{O}_2$  case, several alternative models can be used for mixtures of  $\text{H}_2\text{O}$  and  $\text{CO}_2$  as they occur in the present propellant combination. These are models by Copalle and Johansson. All three simple WSGG models predict almost the same ascent and descent of RWHF whilst there is only small difference in the prediction of the maximum RWHF. The position of the maximum RWHF does not differ significantly between those three models and varies between -0.09 m and -0.07 m which is a difference of 5 % relative to the length of the chamber.

Additionally, the WSGGM by Denison which uses 121 gray gases for two radiating species with the double integration (whose origins are in the use of 10 gray plus 1 clear gas for each species, thus  $11 \times 11 = 121$ ) is in accordance with the three simple models mentioned above. It matches Johansson's results best from the injector down to the throat but differs from the three simple models in the expansion region.

The effort saving simplified options for Denison's WSGGM predict the lowest RWHF that is only half of the other ones' RWHF reaching 0.7 % of the maximum CWHF. A possible reason for the lower prediction of the RWHF with the convolution option is the option's limitation to constant mole fractions which is violated herein. The reason for the lower prediction of Denison's model based on double integration with optimized intervals is that the optimization algorithm yields only one of various local minima instead of the global one. Therefore the results of the three simple models and of Denison's model using 121 gray gases appear more trustworthy since they have neither limitations that are exceeded nor the necessity of optimization.

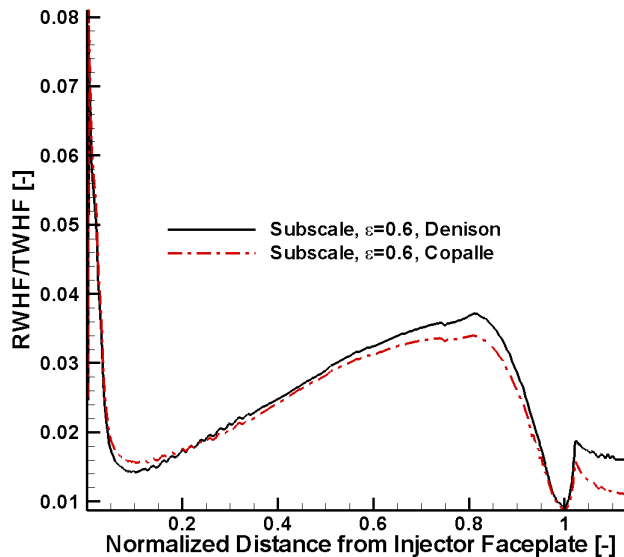


Figure 11: Local influence of RWHF on the TWHF for  $\text{CH}_4/\text{O}_2$  combustion

The local ratio of RWHF to TWHF for two WSGG models at  $\varepsilon=0.6$  is shown in Fig. 11. One can see that the plot is similar to the one for  $\text{H}_2/\text{O}_2$  combustion in the subscale chamber shown in Fig. 7 with the maximum ratio occurring close to the injector. The quantitative level of the ratio of RWHF to TWHF is slightly lower in the  $\text{CH}_4/\text{O}_2$  case reaching a maximum of only 8 % in contrast to 10 % in the  $\text{H}_2/\text{O}_2$  case. The reason for quantitative difference of the ratio is the RWHF which is lower as Fig. 10 underlines.

For the  $\text{CH}_4/\text{O}_2$  combustion, Table 2 shows the integrated ratio of RWHF to TWHF for various WSGG models and emissivities. Similar to the RWHF the integrated RWHF/TWHF is nearly the same for the WSGG models by Smith, Copalle and Denison predicting a maximum ratio of around 2.5 % at  $\varepsilon=0.6$  which is about a half percentage point lower than in the  $\text{H}_2/\text{O}_2$  combustion. For these three models a decrease in emissivity by 0.2 decreases the ratio by 0.8 percentage points. This linear behavior is very similar to the one in the  $\text{H}_2/\text{O}_2$  combustion. The WSGGM by Denison using the double integration option with 121 gray gases yields similar results for  $\varepsilon=0.6$ ; the other emissivities are left out in this work due to the extremely high computational efforts of this method. Nevertheless it can be assumed from the results of the  $\text{H}_2/\text{O}_2$  combustion and from the performances of the other WSGG models in the  $\text{CH}_4/\text{O}_2$  combustion that the reduction with emissivity is comparable.

The integrated ratio gained by the simplified options of Denison's WSGGM is only half of the prediction by the other models because their RWHF is only half of the other models'. Nevertheless, with decreasing emissivity these models behave very similar.

Table 2: Integral ratio of RWHF/TWHF for all WSGG Models and wall emissivities for CH<sub>4</sub>/O<sub>2</sub> combustion

<i>Subscale Chamber</i>	<i>RWHF/TWHF [%]</i>		
	$\epsilon=0.6$	$\epsilon=0.4$	$\epsilon=0.2$
Smith's WSGGM	2.49	1.66	0.83
Copalle's WSGGM	2.55	1.69	0.85
Johansson's WSGGM	2.37	1.55	0.76
Denison's WSGGM (double integration, 121 gases)	2.42	-	-
Denison's WSGGM (double integration, 16 optimized gases)	1.40	0.94	0.47
Denison's WSGGM (convolution, 10 gases)	1.18	0.78	0.39

## 6. Summary & Conclusion

Simulations of radiative heat transfer are carried out for H<sub>2</sub>/O<sub>2</sub> combustion in subscale and fullscale combustion chambers and for CH<sub>4</sub>/O<sub>2</sub> combustion in a subscale combustion chamber. Temperature, pressure and mole fractions of the radiating species H<sub>2</sub>O and CO<sub>2</sub> are imported from Astrium's inhouse CFD code Rocflam-II into the CFD code NSMB that has been utilized to simulate radiative heat transfer. Based on these inputs, NSMB determines parameters for the WSGG models and uses them to solve the P1 radiation transport model. NSMB finally gives the RWHF to the combustion chamber wall which is added to the CWHF given by Rocflam-II to yield the TWHF.

Simulations of the H<sub>2</sub>/O<sub>2</sub> combustion confirm that the RWHF strongly depends on the temperature, reaching a maximum shortly upstream of the location of the maximum cross sectionally averaged temperature. The influence of wall emissivity becomes obvious for that propellant combination as the RWHF decreases linearly with decreasing emissivity of the combustion chamber wall. In relation to the maximum CWHF of each combustion chamber the maximum RWHF is comparable for both subscale and fullscale combustion chambers reaching around 1.7-1.8 % of their maximum CWHF for a wall emissivity of 0.6, which represents a high but still realistic value. The different WSGG models for the H<sub>2</sub>/O<sub>2</sub> combustion have little influence on the RWHF for the subscale chamber whereas for the fullscale chamber the difference between Smith's and Denison's WSGGM increases. This difference in maximum RWHF is caused by the less precise modeling of absorption by Smith's WSGGM. Since the fullscale chamber is five times the diameter of the subscale chamber, the different precision becomes obvious only in this chamber as absorption is overestimated by Smith's model along the increased path length. This decreases the RWHF while increasing the differences between both models and thus revealing the superior accuracy of Denison's WSGGM to Smith's model.

In the H<sub>2</sub>/O<sub>2</sub> combustion, the local ratio of RWHF to TWHF has a maximum shortly downstream of the injector that reaches around 10 %. Further downstream, the ratio decreases and does not exceed 4 % in the rest of the chamber.

The integrated ratio of RWHF to TWHF is around 3 % for the subscale combustion chamber at  $\epsilon=0.6$  and nearly independent on the WSGGM. In the fullscale chamber it is 2.5-3.3 % at  $\epsilon=0.6$ , depending on the WSGG as already mentioned for the maximum RWHF. The integrated ratio decreases linearly by one percentage point when the emissivity is reduced by 0.2 in the subscale combustion chamber and by 0.9 percentage points in the fullscale combustion chamber.

Simulations of the CH<sub>4</sub>/O<sub>2</sub> subscale combustion chamber reveal a similar qualitative behavior of the RWHF over the axial distance, showing similar characteristics as the cross sectionally averaged temperature profile. In that combustion H<sub>2</sub>O and CO<sub>2</sub> are assumed to be radiatively participating. The influence of CO is not considered because up to date WSGG model do not support its spectral properties. The maximum RWHF with respect to the maximum CWHF decreases to 1.65 %. The simple WSGG models by Smith, Copalle and Johansson yield nearly the same RWHF as the sophisticated model by Denison based on double integration and 121 gray gases. The simplified versions of Denison's model, using double integration with 16 optimized gray gases and the convolution approach in order to reduce the computational effort, predict only half of the other models' RWHF. The reason for the difference lies in the fact that the optimization method finds only one of many local minima instead of the global minimum. The convolution approach is valid only for systems with constant mole fractions which is not the case in this work and thus the model is used beyond its limitations.

For decreasing wall emissivities, the decrease of the RWHF is linear, too. The local ratio of RWHF to TWHF for the CH<sub>4</sub>/O<sub>2</sub> combustion behaves similar to the H<sub>2</sub>/O<sub>2</sub> combustion having a slightly reduced maximum of 8 % near the injector faceplate. Throughout the rest of the domain, the ratio of RWHF to TWHF does not exceed 4 % as in the H<sub>2</sub>/O<sub>2</sub> case.

The integrated ratio of RWHF to TWHF decreases for all WSGG models compared to the H<sub>2</sub>/O<sub>2</sub> combustion yielding a maximum of only 2.5 % for  $\epsilon=0.6$ . For lower wall emissivities the ratio then decreases linearly, similar to the behaviour of the maximum RWHF.

The lower RWHF is caused firstly by the lower combustion temperature of the CH<sub>4</sub>/O<sub>2</sub> combustion at the given load point, secondly by the decreased mass fraction of H<sub>2</sub>O and CO<sub>2</sub> whose sum is lower than the mass fraction of single H<sub>2</sub>O in the H<sub>2</sub>/O<sub>2</sub> combustion and thirdly by the lower absolute emissivity of CO<sub>2</sub> compared to H<sub>2</sub>O at the given pressure and temperature levels.

The findings of this work contradict the results of some of the former investigations predicting an integrated ratio of RWHF to TWHF of nearly 8 % for H<sub>2</sub>/O<sub>2</sub> combustion and 9 % for CH<sub>4</sub>/O<sub>2</sub> combustion. Future work will show by detailed comparison to those former investigations that the main reason for the over-prediction is the less profound flow-field of those simulations which does not account for propellant preparation effects near the injector face plate but instead assumes a pre-burnt mixture entering the combustion chamber. By that, the temperature near the injector is overestimated, resulting in an over-prediction of the RWHF and increasing the ratio of RWHF to TWHF. In addition, in the CH<sub>4</sub>/O<sub>2</sub> case the pre-burnt mixture yields a mole fraction of CO<sub>2</sub> that is twice as high as in the current work, increasing the RWHF further as the amount of radiatively participating CO<sub>2</sub> is almost doubled. Finally, by the assumption of a premixed profile, the combustion temperature in general is overestimated as the combustion efficiency is implicitly assumed to be 100%.

In conclusion one can say that it is essential for the prediction of a realistic RWHF to have a realistic flow field including temperature and species distribution. Concerning radiative transport, the P1 model gives satisfactory results. More important appears the spectral modeling: Denison's detailed model shows comparable results to simpler models (i.e. Smith) for small optical path lengths as they appear in the subscale combustion chamber. At bigger path lengths, like in the fullscale chamber, the simpler models show a more pronounced deviation even though the general behavior as well as the order of magnitude is still acceptable. Generally, one has to say that the contribution of gas radiation to the integral heat load of the chamber is relatively small even when assuming an elevated wall emissivity. Consequently, the use of simpler models (i.e. Smith) implying a renouncement of accuracy appears to be acceptable. Future work will also cover the investigation of coupling effects by implementing the divergence of radiative heat flux into the total energy equation of Rocflam-II to account for energy transport by radiation.

## Acknowledgements

The authors gratefully acknowledge support by Martin Göhring and Matthias Thoma who did most of the radiative transfer simulations as part of their Master's theses.

## References

- [1] T. F. Smith, Z. F. Shen, and J. N. Friedman, Evaluation of Coefficients for the Weighted Sum of Gray Gases Model, ASME Journal of Heat Transfer, Vol. 104, pp. 602-608, 1982.
- [2] A. Coppalle, The Total Emissivities of High Temperature Flames, Combustion and Flame, Vol.49, pp. 101-108, 1983.
- [3] M. K. Denison and B. W. Webb, An Absorption-Line Blackbody Distribution Function for Efficient Calculation of Total Gas Radiative Transfer, Journal of Quantitative Spectroscopy & Radiative Transfer, Vol. 50, pp.499-510, 1993.
- [4] R. Johansson, Account for Ratios of H<sub>2</sub>O to CO<sub>2</sub> in the Calculation of Thermal Radiation of Gases with the Weighted-Sum-of-Grey-Gases Model, Proceedings of the Sixth Mediterranean Combustion Symposium, 2009.
- [5] J. B. Vos, A. W. Rizzi, A. Corjon, E. Chaput, and E. Soinnie, Recent advances in aerodynamics inside the NSMB (Navier Stokes Multi Block) consortium, Aerospace Sciences Meeting and Exhibit, 36th, Reno, 1998.
- [6] F. Göbel and Ch. Mundt, Implementation of the P1 Radiation Model in the CFD solver NSMB and Investigation of Radiative Heat Transfer in the SSME Main Combustion Chamber, 17th AIAA International Space Planes and Hypersonic Systems and Technologies Conference, 2011.
- [7] M. H. Naraghi, S. Dunn, S. and D. Coats, Modeling of Radiation Heat Transfer in Liquid Rocket Engines, AIAA-2005-3935, Joint Propulsion Conference, Arizona, 2005.
- [8] T.-S. Wang, Unified Navier-Stokes Flowfield and Performance Analysis of Liquid Rocket Engines, 1990.

- [9] A. Thellmann, Impact of Gas Radiation on Viscous Flows, in particular on Wall Heat Loads, in Hydrogen-Oxygen vs. Methane-Oxygen Systems, based on the SSME Main Combustion Chamber, Universität der Bundeswehr München, PhD Thesis, Institute of Thermodynamics, 2010.
- [10] F. Göbel, D. Birgel, and A. Thellmann, CFD Simulation of Hydrogen-Oxygen and Methane-Oxygen System for Space Shuttle Main Combustion Chamber including Radiative Effects, 60th International Astronautical Congress, 2009.
- [11] M. Frey , Th. Aichner , J. Görden , B. Ivancic , B. Kniesner , O. Knab, Modeling of Rocket Combustion Devices, 10th AIAA/ASME Joint Thermophysics and Heat Transfer Conference, Chicago, IL, 2010.
- [12] R. Siegel and J. R. Howell, Thermal Radiation Heat Transfer, McGraw-Hill, Tokyo et al., 1972.
- [13] M. F. Modest, Radiative Heat Transfer, Second Edition ed., Academic Press, San Diego (USA), London (UK), Burlington (USA), 2003.
- [14] F. Göbel, Implementation of Spectral Models for Gas Radiation into the CFD Solver NSMB and Validation on the basis of the SSME Main Combustion Chamber, Diploma Thesis, Institute of Thermodynamics, Universität der Bundeswehr München, 2009.
- [15] Denison, M. K. and Webb, B. W., An absorption line blackbody distribution function for efficient calculation of total gas radiative transfer, Journal of Quantitative Spectroscopy and Radiative Transfer, Vol. 50, No. 5, pp. 499-510, 1993.
- [16] M.K. Denison and B.W. Webb, The Spectral-Line Weighted-Sum-of-Gray-Gases Model for H<sub>2</sub>O/CO<sub>2</sub> Mixtures, Journal of Heat Transfer, Vol. 117, No. 3, pp. 788-792, 1995.
- [17] M. Thoma, Numerische Untersuchung der ungekoppelten Gasstrahlung in einer CH<sub>4</sub>/O<sub>2</sub> Raketenbrennkammer, Institute of Thermodynamics, Universität der Bundeswehr München, 2009.
- [18] J. Görden, Th. Aichner and M. Frey, Spray Combustion and Heat Transfer Modelling in LOX/H<sub>2</sub>, LOX/HC and MMH/NTO Combustion chambers, 3rd European conference for Aerospace Sciences (EUCASS), Versailles, France, 2009.
- [19] B. Kniesner, M. Frey, O. Knab, Numerical Investigation of Gas Generator and Preburner Flows for Rocket Engine Applications, 4th European Conference for Aerospace Sciences (EUCASS), St. Petersburg, Russia, 2011.